Integrating thermal stress indexes within Shuttleworth–Wallace model for evapotranspiration mapping over a complex surface

Jamal Elfarkh, Salah Er-Raki, Jamal Ezzahar, Abdelghani Chehbouni, Bouchra Aithssaine, Abdelhakim Amazirh, Saïd Khabba, Lionel Jarlan

Irrigation Science
https://doi.org/10.1007/s00271-020-00701-3

ORIGINAL PAPER

Integrating thermal stress indexes within Shuttleworth–Wallace model for evapotranspiration mapping over a complex surface

Jamal Elfarkh[1] · Salah Er-Raki[1,2] · Jamal Ezzahar[2,3] · Abdelghani Chehbouni[2,4] · Bouchra Aithssaine[2] · Abdelhakim Amazirh[2] · Saïd Khabba[2,5] · Lionel Jarlan[4]

Received: 31 December 2019 / Accepted: 18 September 2020

Abstract

The main goal of this work was to evaluate the potential of the Shuttleworth–Wallace (SW) model for mapping actual crop evapotranspiration (ET) over complex surface located in the foothill of the Atlas Mountain (Morocco). This model needs many input variables to compute soil (r_s^s) and vegetation (r_s^v) resistances, which are often difficult to estimate at large scale particularly soil moisture. In this study, a new approach to spatialize r_s^s and r_s^v based on two thermal-based proxy variables was proposed. Land Surface Temperature (LST) and Normalized Difference Vegetation Index (NDVI) derived from Landsat data were combined with the endmember temperatures for soil (Ts_{min} and Ts_{max}) and vegetation (Tv_{min} and Tv_{max}), which were simulated by a surface energy balance model, to compute the soil (Ts) and the vegetation (Tv) temperatures. Based on these temperatures, two thermal proxies (SI_{ss} for soil and SI_{sv} for vegetation) were calculated and related to r_s^s and r_s^v, with an empirical exponential relationship [with a correlation coefficient (R) of about 0.6 and 0.5 for soil and vegetation, respectively]. The proposed approach was initially evaluated at a local scale, by comparing the results to observations by an eddy covariance system installed over an area planted with olive trees intercropped with wheat. In a second step, the new approach was applied over a large area which contains a mixed vegetation (tall and short) crossed by a river to derive r_s^s and r_s^v, and thereafter to estimate ET. A Large aperture scintillometer (LAS) installed over a line transect of 1.4 km and spanning the total area was used to validate the obtained ET. The comparison confirmed the ability of the proposed approach to provide satisfactory ET maps with an RMSE, bias and R^2 equal to 0.08 mm/h, 0.06 mm/h and 0.80, respectively.

Introduction

The fast-growing population and economy in recent decades are accompanied by an increase in agricultural production. Agricultural and irrigation techniques have been widely developed, but the deterioration and depletion of water resources remain a problem that threatens the future of food security, especially in arid and semi-arid zones (Plattner et al. 2009; Gohar et al. 2019). Rational management of water resources, which is a primary concern for the managers, requires a good knowledge of the water and energy processes taking place in the soil-vegetation-atmosphere continuum (Blinda 2012; Bhattarai et al. 2019). Indeed, the control of these processes allows to assess the exact amount of water that the plant requires overtime, which is similar to the field water loss through evapotranspiration (Allen et al. 2011). The process of evapotranspiration is difficult to determine because of various challenges, including the vegetation complexity, plant diversity, lack of available data and because the in-situ direct measurement of ET is difficult

✉ Salah Er-Raki
s.erraki@uca.ma; s.erraki@gmail.com

[1] ProcEDE, Département de Physique Appliquée, Faculté des Sciences et Techniques, Université Cadi Ayyad, Marrakech, Morocco

[2] Mohammed VI Polytechnic University (UM6P), Center for Remote Sensing Applications (CRSA), Ben Guerir, Morocco

[3] Département IRT, Laboratoire MISCOM, Ecole Nationale des Sciences Appliquées, Université Cadi Ayyad, Safi, Morocco

[4] Centre d'Etudes Spatiales de La BIOsphère, Toulouse, France

[5] LMFE, Département de Physique, Faculté des Sciences Semlalia, Université Cadi Ayyad, Marrakech, Morocco

Journal : Large 271 | Article No : 701 | Pages : 17 | MS Code : 701 | Dispatch : 30-9-2020

in complex surfaces like our study site. Then an accurate assessment of evapotranspiration (ET) is crucially needed at the basin scale for studying the hydrological processes and water balance especially from upstream to downstream and it is required for a good integrated water management. There is thus an imperative need to develop reliable computation method with a limited number of input parameters especially over complex surfaces.

Several methods have been used to measure ET and its components [plant transpiration (T) and soil evaporation (E)], which are different in complexity and/or in accuracy. The principles of these methods are various; they can be hydrological, physiological or micrometeorological. Based on the hydrological balance, the lysimeter provides direct evaporation or evapotranspiration measurements at a local scale and over homogeneous canopy (Allen et al. 2011; Sánchez et al. 2019). To assess the plant transpiration, the physiological approach has been used based on introducing a source of low-grade heat into the stem or the trunk of a plant. This approach known as the sap flow method, can be used in homogeneous crops but it requires an up-scaling procedures to extrapolate measurements from individual plants to the stand level transpiration (Green et al. 2003; Steppe et al. 2010; Er-Raki et al. 2010a; Rafi et al. 2019). Currently, around the world the micrometeorological techniques such as eddy covariance are widely used to measure ET over a scale of a few hectares, depending on the height of the measurements (Ezzahar et al. 2007; Allen et al. 2011; Fang et al. 2020). By contrast, the scintillometer technique that was recently developed allows for measurements of sensible (optical LAS) and latent (microwave LAS) heat fluxes over transects up to 10 km (Ezzahar and Chehbouni 2009; Ezzahar et al. 2009b, a; Zieliński et al. 2013, 2017; Yee et al. 2015). In addition, scintillometers are easy to install, to monitor and can provide measurements of the surface fluxes over complex surfaces which makes them suitable for validating remote sensing-based methods (Duchemin et al. 2008; Tang and Li 2015; Huang et al. 2016; Ait Hssaine et al. 2018; Saadi et al. 2018). The LAS applies the Monin–Obukhov Similarity Theory (MOST) to estimate the sensible heat flux. However, the applicability of MOST is limited when conditions are not favorable, which can happen for a number of reasons. Atmospheric conditions, instrumental setup, data processing and evaluation criteria (particularly choice of similarity function and variable of interest) can all affect the MOST applicability (Ward 2017).

With regard to modelling aspect, there are different types of models to estimate surface fluxes. They range from complex physically based, conceptual, to empirical ones. There are some models characterised by a simplified relation using thermal infrared and micrometeorological data (Jackson et al. 1977; Seguin and Itier 1983). Others are based on residual methods of the energy budget (Surface Energy Balance Algorithm for Land (Bastiaanssen et al. 1998), Surface Energy Balance System (Su 2002), two-source energy balance (Norman et al. 1995), Mapping Evapotranspiration at a high-Resolution with Internalized Calibration (Allen et al. 2007)). A third one, more complex, characterizes the energy and water transfers in all the continuum soil-vegetation-atmosphere (Interaction Soil Biosphere Atmosphere (Noilhan and Mahfouf 1996; Aouade et al. 2020), Simple Soil-Plant-Atmosphere Transfer (Braud et al. 1995), Soil Plant Atmosphere and Remote Sensing Evapotranspiration (Boulet et al. 2015) and the Interactive Canopy Radiation Exchange (Gentine et al. 2007)). Compared to those based only on the energy budget, this category of models needs more input data which is often not available at large scale. Finally, some other approaches use a crop coefficient to provide actual ET from reference or potential one (Allen et al. 2005; Neale et al. 2005). These models can be extended to large areas when they are combined with remote sensing data (Duchemin et al. 2008; Er-Raki et al. 2010b; Diarra et al. 2017). Satellite products such as land surface temperature (LST), emissivity, albedo and vegetation indexes have been improving in their spatiotemporal resolution during the recent years, especially with the launch of Landsat 7 and 8 and Sentinel 2 satellites. Consequently, mapping and assessing ET over heterogeneous and large areas became a promising challenge which has been largely investigated in recent years (Albergel 2010; Singh et al. 2014; Semmens et al. 2016; Tan et al. 2019).

The two components of the ET are influenced differently by many factors which mean that the contribution of each one (E and T) to the total ecosystem ET is highly variable in time and space (Aouade et al. 2016). Consequently, estimating accurate ET over vegetation canopy using two-source models is necessary since this type of model computes each component distinctly. In this context, Shuttleworth and Wallace developed in Shuttleworth and Wallace 1985 a two-source model taking into account the interaction flux from vegetation and soil separately. It is characterized by a rigorous physically based framework which provides accurate ET estimation values especially for row crops (Ortega-Farias et al. 2007; Zhang et al. 2008). However, Shuttleworth–Wallace (SW) model is significantly sensitive to errors in the values of soil and vegetation resistances (Zhu et al. 2014). These resistances can be parameterized using measurements of E, T and ET (Samanta et al. 2007; Villagarcía et al. 2010; Zhu et al. 2014). Many authors have used empirical equations to compute these resistances based on surface and root-zone soil water content (Ramírez et al. 2007; Were et al. 2007). However, the soil water content is difficult to obtain at a large scale. Several methods were developed to estimate this variable but they are complex and need the knowledge of many physical soil parameters (Guswa et al. 2002; Verhoef et al. 2006; Merlin et al. 2016). For this reason and to

Journal : Large 271 | Article No : 701 | Pages : 17 | MS Code : 701 | Dispatch : 30-9-2020

estimate spatial values of ET using the SW model, a parameterization of the soil and vegetation resistances using a thermal-based proxy derived from Landsat was proposed in this paper. The stress indexes presented by this proxy reflect the hydric state of both soil and vegetation since the temperature variation of the soil or the vegetation can be attributed to change in the water content between dry and wet conditions. In this context, good results have been obtained by relating thermal-based proxy of vegetation water stress to canopy resistance (Amazirh et al. 2017) and to stress coefficient in FAO-56 (Olivera-Guerra et al. 2018, 2020). The novelty of the proposed approach is the link of both vegetation and soil resistances to the stress indexes which can provide an accurate estimation of spatial ET.

This paper is organized as follows: first, an overview of the study area, the experimental design and the proposed approach is presented. After, a description of the obtained results at a local scale is provided. Then, an illustration of the spatial results with a discussion about the potential of the developed approach to assessing the evapotranspiration over a heterogeneous semi-arid region is presented. Finally, a summary and conclusions are provided.

Materials and methods

Study area and data description

Study area description

An experiment was conducted over the piedmont of the Atlas mountain in the center of Morocco (Tahanaout city, Fig. 1). This area is characterized by a semi-arid climate with a low annual rainfall amount especially for 2017 where an annual cumulative value of about 157 mm compared to the cumulative value during last two decades (302 mm). The land use mapping of the experimental area is also presented in Fig. 1a. According to this figure, one can remark clearly that the area is heterogeneous and composed of small fields planted by olive trees with a height ranging from 3 to 12 m which were measured using the 45° Triangle method (Fig. 1b). Note that some farmers mix the olive trees with herbaceous crops such as wheat, alfalfa and/or corn. In the same area apricot, plum, orange and peach trees are also cultivated. The bare soil is mainly present on the sides of Rherhaya river and on the North-West part of the study area. Additionally, the heterogeneity of the site is amplified by the difference in the height between different trees and herbaceous crops. All fields are irrigated using the flooding technique. In general, the irrigation water comes from mountain (rainfall or melting snow) and is diverted to the study area through traditional networks (Bouimouass et al. 2020).

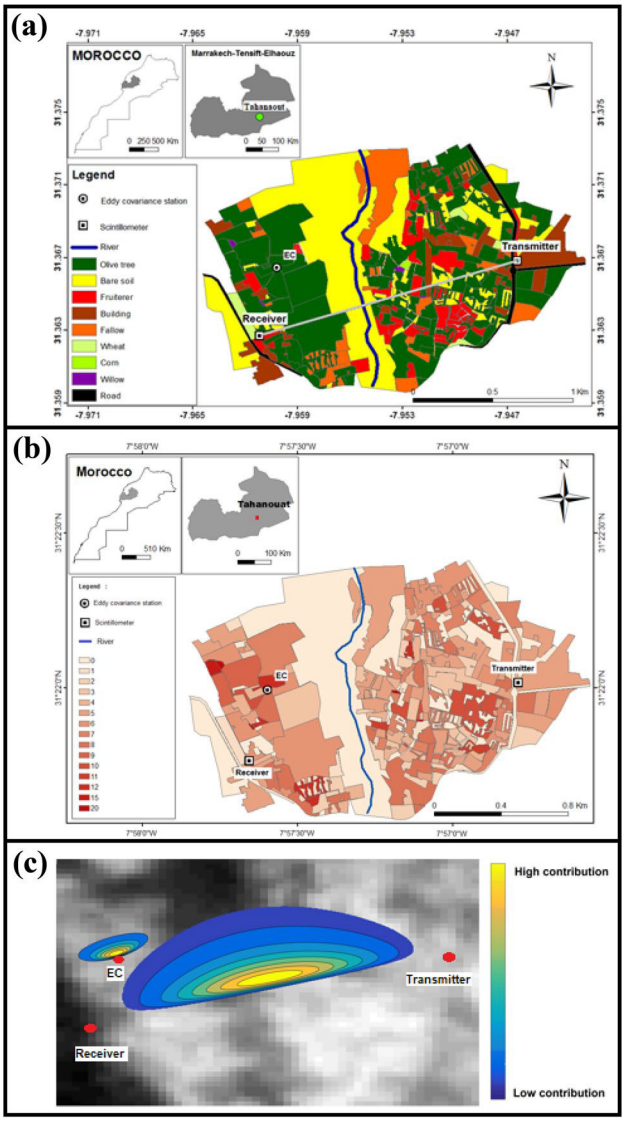

Fig. 1 Locations of the Eddy Covariance (EC) station, the scintillometer (transmitter and receiver) superimposed on the land use map (**a**), vegetation height map (**b**) and Landsat image with their footprint (**c**)

Meteorological data, eddy covariance and scintillometer measurements

A set of instruments was deployed over the EC tower in the study site for measuring meteorological data, turbulent fluxes, soil moisture and surface temperature. Air temperature and humidity were measured with a Vaisala (HMP155, Campbell scientific) at a height of about 15.6 m. The four components of the net radiation were measured using a CNR4 radiometer (Campbell scientific) at a height of about 16.7 m. The soil heat flux was averaged using the measurement of two heat flux plates at 5 cm depths (HPF01, Hukseflux) in two locations: one below the tree (always shaded) and the other between the trees (directly exposed to solar

radiation). Soil moisture was measured at different depths (5 and 15 cm) using CS655 water content reflectometers (Campbell Scientific). Radiometric brightness temperature was measured over the soil and the vegetation separately using an Infra-Red radiometer (IRTS-P's, Apogee) and then converted to land surface temperature (LST) using surface emissivity. One of the radiometers was positioned at height of about 11.7 m directed vertically towards the ground and the other one was positioned at height of about 6.5 m directed towards the vegetation with a view angle of about 60 degrees. An eddy covariance (EC) system was installed on 17.5 m height tower to measure the latent and sensible heat fluxes. It is composed of a three-dimensional sonic anemometer (CSAT3, Campbell Scientific Ltd.) and a Krypton hygrometer (KH20, Campbell Scientific Ltd.). Raw data were sampled at a rate of 20 Hz and processed using the ECpack software to compute turbulent fluxes. The comparison between available energy ($\mathrm{Rn} - G$) and the sum of the sensible (H) and latent (LE) heat fluxes shows a non-closure of the energy balance which is expected given the high complexity of the surface. The turbulent flux values used in this work were corrected using the approach proposed by (Twine et al. 2000) which is based on the hypothesis that the ratio H/LE is accurately measured than H and LE separately. Then, corrected turbulent fluxes were derived as $\mathrm{LE} = \frac{\beta}{\beta+1}(\mathrm{Rn} - G)$ and $H = \frac{(Rn-G)}{\beta+1}$, with β computed from the 30-min observed H and LE. Additionally, a Large Aperture Scintillometer (LAS) was set up over a 1464 m transect spanning a representative area of the total site across the river between 10 and 50 m above the ground, with an effective height of ≈ 26 m. It consists of a transmitter installed at a height of 10.5 m and a receiver mounted at the height of 10 m (Fig. 1). Measurements were sampled at 1 Hz, averaged, and then stored at 30 min intervals on CR10X dataloggers. In this study, a footprint model proposed by Horst and Weil (1992, 1994) was applied to average the remote sensing data over the source areas where the turbulent fluxes were emanated (see Appendix 1).

Remote sensing data

In this study, 17 satellite images were collected from Landsat 7 and 8. Combining the two satellites, a repeatability of eight days was reached. The resolution of the acquired images ranges from 30 to 100 m, depending on the spectral bands. The satellites products were downloaded from the USGS website (https://earthexplorer.com/). Nevertheless, the radiation measured by Landsat 7/8 has to be corrected from the atmosphere. To overcome this issue and derive actual land surface temperature (LST), the images were corrected following the steps described in Tardy et al. (2016). The corrections associated with the radiation emitted by the atmosphere and to the atmospheric attenuation were based on the vertical atmospheric conditions (pressure, temperature, water vapor and ozone) of the ERA-Interim dataset. The atmospheric correction parameters were finally computed using the commercial RTM software MODTRAN. The surface emissivity was determined based on the vegetation index (NDVI) according to Wittich (1997).

Evapotranspiration modelling

Shuttleworth–Wallace model

Shuttleworth and Wallace developed a parameterization of the canopy evapotranspiration in 1985. This model considers two sources of water transfer from the surface to the atmosphere, from the soil by the evaporation process and from the vegetation through transpiration. For each source, the model takes into account both aerodynamic and surface resistances and assumes that the two sources will interact at the effective canopy's height considering another aerodynamic resistance between this height and the reference height source. The model is represented as follows:

$$\mathrm{ET} = \mathrm{E} + \mathrm{T} = C_\mathrm{s}\mathrm{PM}_\mathrm{s} + C_\mathrm{v}\mathrm{PM}_\mathrm{v} \tag{1}$$

where E is the soil evaporation, T is the vegetation transpiration, $\mathrm{PM_s}$ and $\mathrm{PM_v}$ are terms similar to the Penman–Monteith combination equation.

They are expressed by the two following equations:

$$\mathrm{PM_s} = \frac{\Delta A + \left[\left(\rho C_\mathrm{p} D - \Delta\, r_\mathrm{a}^\mathrm{s}\left(A - A_\mathrm{s}\right)\right)/\left(r_\mathrm{a} + r_\mathrm{a}^\mathrm{s}\right)\right]}{\Delta + \gamma\left[1 + r_\mathrm{s}^\mathrm{s}/\left(r_\mathrm{a} + r_\mathrm{a}^\mathrm{s}\right)\right]} \tag{2}$$

$$\mathrm{PM_v} = \frac{\Delta A + \left[\left(\rho C_\mathrm{p} D - \Delta\, r_\mathrm{a}^\mathrm{v}\left(A - A_\mathrm{s}\right)\right)/\left(r_\mathrm{a} + r_\mathrm{a}^\mathrm{v}\right)\right]}{\Delta + \gamma\left[1 + r_\mathrm{s}^\mathrm{v}/\left(r_\mathrm{a} + r_\mathrm{a}^\mathrm{v}\right)\right]} \tag{3}$$

where A and A_s are the available energy above canopy and the soil surfaces ($\mathrm{W/m^2}$), respectively. Δ is the slope of saturation vapour pressure curve (kPa/K), ρ is the air density ($\mathrm{kg/m^3}$), C_p is the specific heat of dry air at constant pressure (J/kg/K), D is the water vapor deficit (kPa), γ is the psychrometric constant (Pa/K).

The coefficients C_s and C_v are given as follows:

$$C_\mathrm{s} = \frac{1}{1 + \left[R_\mathrm{s}R_\mathrm{a}/R_\mathrm{v}\left(R_\mathrm{s} + R_\mathrm{a}\right)\right]} \tag{4}$$

$$C_\mathrm{v} = \frac{1}{1 + \left[R_\mathrm{v}R_\mathrm{a}/R_\mathrm{v}\left(R_\mathrm{v} + R_\mathrm{a}\right)\right]} \tag{5}$$

where R_s, R_v, R_a are formulated as:

$$R_s = (\Delta + \gamma) r_a^s + \gamma r_s^s \quad (6)$$

$$R_v = (\Delta + \gamma) r_a^v + \gamma r_s^v \quad (7)$$

$$R_a = (\Delta + \gamma) r_a \quad (8)$$

where r_a^v, r_a, and r_a^s are the aerodynamic resistance of the canopy, the aerodynamic resistance between the reference height and the effective height and from the effective height to the soil surface (s/m), respectively. Additionally, soil evaporation and plant transpiration are controlled by the soil surface resistance (r_s^s) and the canopy resistance (r_s^v), respectively. Both resistances are expressed as follow:

$$r_s^s = r_{s\,\min}^s \left(2.5 \left(\frac{\theta_F}{\theta_s} \right) - 1.5 \right) \quad (9)$$

$$r_s^v = \frac{r_{STmin}}{\mathrm{LAI} \prod_{i=1}^{3} F_i(X_i)} \quad (10)$$

$$F_1(S) = \left(\frac{S}{1100} \right) \left(\frac{1100 + a_1}{S + a_1} \right) \quad (11)$$

$$F_2(T) = \frac{(T - T_L)\,(T_H - T)^{(T_H - a_2)/(a_2 - T_L)}}{(a_2 - T_L)\,(T_H - a_2)^{(T_H - a_2)/(a_2 - T_L)}} \quad (12)$$

$$F_3(\theta) = \begin{cases} 1, \theta \geq \theta_F \\ \frac{\theta - \theta_W}{\theta_F - \theta_W}, \theta_W < \theta < \theta_F \\ 0, \theta \leq \theta_W \end{cases} \quad (13)$$

where $r_{s\min}^s$ is the minimum soil surface resistance (taken as 100 s/m (Zhang et al. 2008)) and r_{STmin} is the minimal stomatal resistance of individual leaves under optimal conditions (taken as 146 s/m (Zhang et al. 2008)). θ_s is the water content of the upper soil surface layer (cm^3/cm^3). LAI is the leaf area index, and $F_i(X_i)$ is the stress function of the incoming photosynthetically active radiation flux (S), the air temperature (T) and the actual soil moisture content in the root-zone (θ). T_H and T_L are the upper and lower temperature limits outside of which transpiration is assumed to stop (°C) and are set at values of 40 and 0 °C (Harris et al. 2004). θ_W is the soil moisture content at wilting point (cm^3/cm^3), θ_F is the soil water content at field capacity (cm^3/cm^3). The empirical coefficients a_1 and a_2 were derived by optimization and were set to 57.67 and 25.78 (Zhang et al. 2008), respectively.

The available energies above canopy and above the soil surface are defined by the following expressions: where G is the soil heat flux (W/m^2) and Rn is the net radiation (W/m^2).

$$A = \mathrm{Rn} - G \quad (14)$$

$$A_s = \mathrm{Rn}_s - G \quad (15)$$

Rn_s is the net radiation fluxes into the soil surface (W/m^2) which is parametrized as follows: where C is the extinction coefficient of light attenuation, that equal to 0.68 for the fully grown plant (Sene 1994). Moreover, resistance parameterizations are detailed in Zhang et al. (2008).

$$\mathrm{Rn}_s = \mathrm{R}_n e^{-C \times \mathrm{LAI}} \quad (16)$$

Leaf area index (LAI) is derived from Landsat NDVI following Wang et al. (2008):

$$\mathrm{LAI} = \begin{cases} 0, \ \mathrm{NDVI} < 0.2 \\ \sqrt{\mathrm{NDVI} \frac{1 + \mathrm{NDVI}}{1 - \mathrm{NDVI}}}, \ \mathrm{NDVI} \geq 0.2 \end{cases} \quad (17)$$

Energy balance model and hourglass method

Soil energy balance model: The soil energy balance model was implemented to compute the endmembers temperature (Ts_{min}, Ts_{max}, Tv_{min} and Tv_{max}) further used in the Hourglass method. The extremes soil temperature Ts_{min} and Ts_{max} were simulated by forcing the surface resistances to 0 and ∞, respectively (Stefan et al. 2015; Merlin et al. 2016; Amazirh et al. 2017, 2018). The model was initialized by the observed air temperature and soil temperature is sought by minimizing the following cost function F: where H and LE are the sensible and latent heat fluxes, respectively.

$$F = (\mathrm{Rn} - G - H - \mathrm{LE})^2 \quad (18)$$

The Tv_{min} was set to the air temperature measured over the studied areas (Carlson et al. 1995; Bastiaanssen et al. 1998; Roerink et al. 2000; Merlin 2013; Stefan et al. 2015). For Tv_{max}, it was defined according to the assumptions described in Stefan et al. (2015), which considered the differences between the extreme soil temperatures is the same that between the extreme vegetation temperatures.

Hourglass method: Based on the strong relationship between the variation of the cover fraction (fc) and the surface temperature (LST), Moran et al. (1994) determined a polygon with four zones where each one is characterized by a range of values of fc and LST. Merlin et al. (2012) defined and separated four zones: transpiration- and evaporation-controlled, stressed and unstressed mixed surface. The endmembers obtained with the soil energy balance were used in the Hourglass method to determine the four zones. Hereafter, the partitioning of LST into its soil and vegetation components is based on the LST and fc within the polygon to determine one of the temperature components T_v or T_s (see Appendix 2).

Soil and vegetation temperature estimations: A time series of vegetation and soil temperatures (T_v and T_s) and their

Journal : Large 271 | Article No : 701 | Pages : 17 | MS Code : 701 | Dispatch : 30-9-2020

corresponding endmembers (Ts_{min}, Ts_{max}, Tv_{min} and Tv_{max}) from day of the year 45–60 (2017) are shown in Fig. 2. In this section, LST used in Eq. 32 was inverted from the longwave radiation emitted by the surface and measured using CNR4 as follow:

$$\mathrm{LST} = \left(\frac{\mathrm{LW}}{\varepsilon\sigma}\right)^{1/4} \tag{19}$$

where LW is the longwave radiation emitted by the surface, ε is the surface emissivity and σ is the Stefan-Boltzmann constant. This period was chosen to illustrate the variation of the different temperatures since it coincides with the development stage of the wheat that presents a mixture of soil and vegetation. The two temperatures T_v and T_s ranged between their minimum and maximum values supporting the good performances of the Hourglass method. To validate the two components T_v and T_s of the partition of the LST, both were compared against soil and vegetation temperature observations (Fig. 3). T_v is well reproduced with an RMSE and R^2 equal to 1.6 K and 0.94, respectively. By contrast, the simulated T_s is not as good with an RMSE and R^2 of about 3 K and 0.76, respectively. It is clearly seen that both temperatures T_s and T_v are overestimated, with a bias equal to -1.4 K and -1 K for T_s and T_v, respectively. This scattering can be justified by numerous factors. As T_v was computed first for most of the time while T_s was deducted from Eq. 32. Meaning that T_s accumulated errors of both T_v and LST. Likewise, the discrepancy can be related to the estimation of *fc* from Landsat NDVI, as the Landsat pixel size is larger than the surface of view of the IRT-Apogee. This will obviously lead to some errors in the partition of temperature between soil and vegetation. Another reason that can probably explain the discrepancy is the location of the measurements. As reported by Olivera-Guerra et al. (2018) the youngest leaves of the plant are expected to be

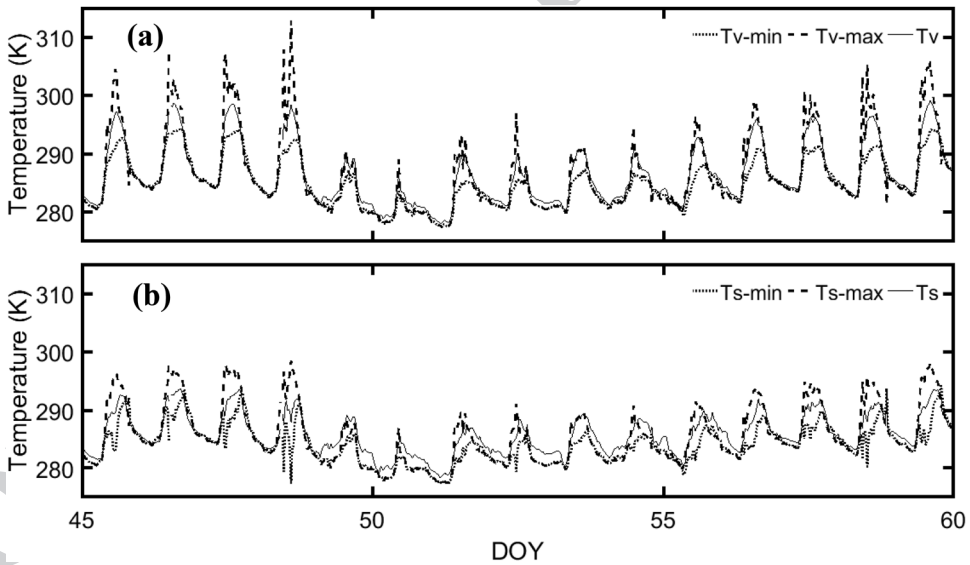

Fig. 2 Variation of soil (**a**) and vegetation (**b**) temperatures derived from Hourglass method, and their maximum and minimum computed from soil surface energy balance model, from DOY 45 to DOY 60

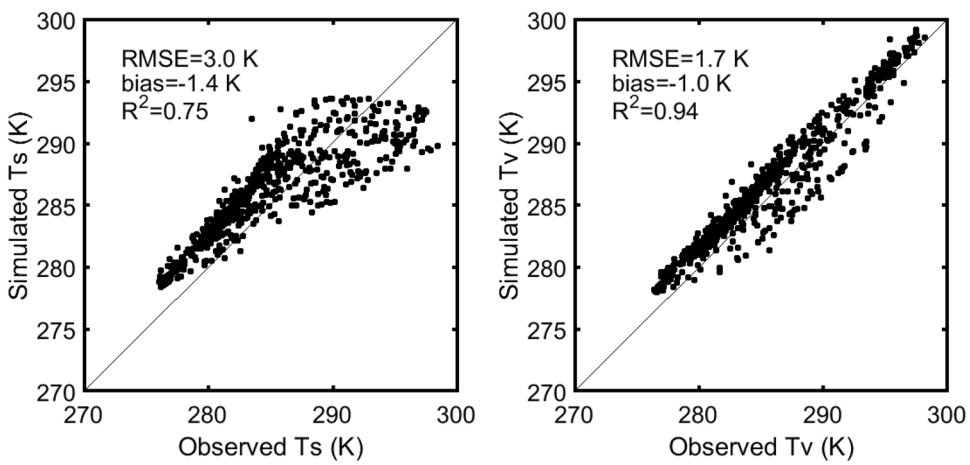

Fig. 3 Simulated soil and vegetation temperatures versus in situ measurements for the same period as Fig. 2

colder than the adult and senescing leaves, whose temperature has not been measured. Otherwise, by comparing both simulated T_s and T_v temperatures in terms of magnitude it can notice that T_v is superior to T_s. T_s never exceeds 294 K although T_v reaches 300 K. This can be explained by the plotting period of T_s and T_v that coincides with the development stage of wheat planted under olive trees and thus there was no bare soil surface. As well as, T_s can be lower than T_v during rainfall or irrigation events. Overall, these results are in agreement with the values reported in the literature (Stefan et al. 2015; Olivera-Guerra et al. 2018). Soil and vegetation temperatures and their endmembers are used to calculate the two stress indexes related to the soil (SI_{ss}) and to the vegetation (SI_{sv}), and finally to estimate spatial ET by the SW model.

Spatialization of the SW model

ET derived by the SW model showed a good consistency at the local scale (Zhang et al. 2008; Zhu et al. 2013, 2014). However, to our knowledge, no study tried to spatialize the SW model since many variables are required especially, for the soil and the vegetation resistances (r_s^s and r_s^v) computation. As mentioned above, this work aims to retrieve the resistances using accurate values of transpiration and evaporation and to suggest a relationship between the retrieved resistances and the stress indexes based on the measured LST. In fact, retrieving these resistances from measurements based on the equations of the SW model is very difficult mathematically. To overcome this issue, the Shuttleworth–Wallace model has been used to retrieve the two resistances values based on a very small threshold convergence (less than 2 W/m^2) defined as the absolute value of the difference between simulated (ET_{SW}) and measured (ET_{EC}) evapotranspiration. This threshold is chosen based on the reliability of the simulated values and on their number to get enough points to develop the relationship between the indices and the resistances. Hereafter, an empirical exponential relationship was developed between the retrieved resistances and the soil and the vegetation stress indexes (SI_{ss}, SI_{sv}). These latter were computed using the endmember temperatures deducted from the soil energy balance model and the vegetation and the soil temperature calculated using Hourglass method as follow:

$$SI_{ss} = \frac{Ts - Ts_{min}}{Ts_{max} - Ts_{min}} \quad (20)$$

$$I_{sv} = \frac{Tv - Tv_{min}}{Tv_{max} - Tv_{min}} \quad (21)$$

An overview of the methodology is summarized in Fig. 4.

Results

In situ evaluation of the SW model

Figure 5 presents a comparison between the half-hourly ET measured by eddy covariance system (average of 0.26 mm/h) and simulated (average of 0.30 mm/h) by the original SW model based on the soil moisture data to compute soil and

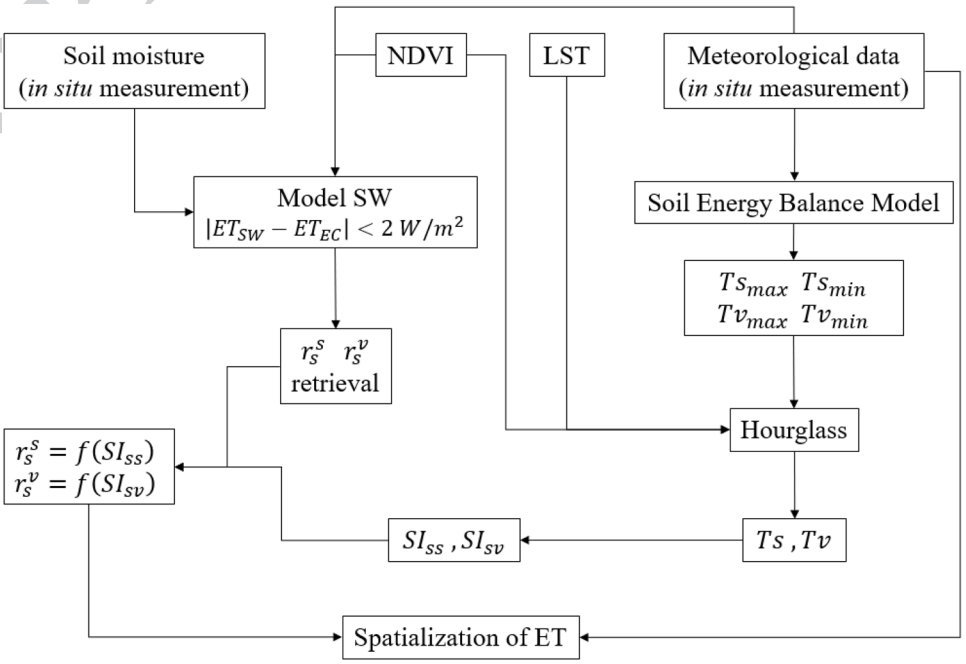

Fig. 4 Flowchart of the proposed approach

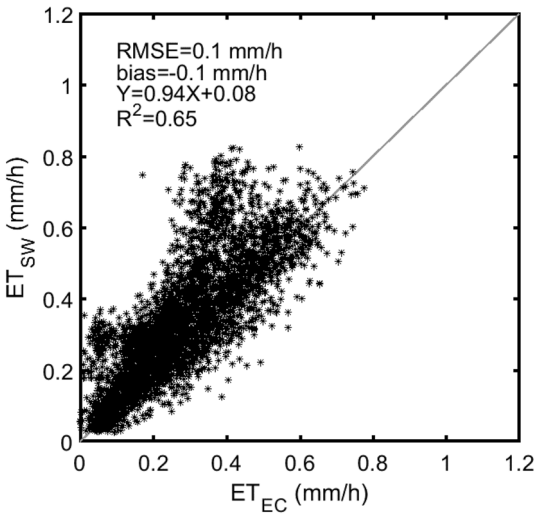

Fig. 5 Half-hourly comparison between evapotranspiration predicted by the Shuttleworth–Wallace model (ET_{SW}) and measured by the Eddy covariance system (ET_{EC}) during 2017

vegetation resistances, during the 2017 growing season. This figure shows that the linear regression between simulated and in situ ET is very encouraging with a slope and an intercept of about 0.94 and 0.08 mm/h, respectively. According to the statistical analysis depicted in this figure, the model simulations are acceptable with a relative RMSE, bias and R^2 of about 0.38, −0.1 mm/h and 0.65, respectively. The obtained results indicate that the model is able to predict ET over surface with a high degree of canopy cover heterogeneity. The scatter of modeled ET is mainly due to canopy uniformity over the surface. Moreover, the experimental plot is irrigated differently during the season. In fact, the farmer irrigates the entire surface when the wheat was cultivated under the olive trees. By contrast, when there is no wheat, the irrigations were limited to the tree rows. This can create a large heterogeneity over the EC footprint. Additionally, this heterogeneity can affect the soil and vegetation resistances which were estimated using data acquired near the EC tower. Another major issue that can explain the differences between measured and simulated ET is the non-closure of the energy balance at the EC system level. The comparison between the available energy and the turbulent fluxes shows that the sum of the turbulent fluxes only reaches 60% of the available energy. This non-closure is similar to what has been observed in previous studies (Mauder et al. 2006; Liu et al. 2011) and can be considered acceptable due to the complexity of the study site. In fact, the EC measurements were corrected using Bowen ratio method (Twine et al. 2000). However, the correction was not ideal due to the storage and the photosynthesis terms which were not taken into consideration. Additionally, the footprint devices of the EC system, the CNR4 radiometer and the soil flux plaques were quite different. Furthermore, the soil heat flux was measured using a heat flux plate, which does not take into consideration the heat storage in the soil layer above it. This error related to the G measurements can affect the Bowen correction of the EC measurements and consequently the comparison between simulated and measured ET.

As reported by Zhang et al. (2009), when the soil was partially wetted the SW model tends to overestimate ET by 25.2% over a vineyard. Likewise, Zhang et al. (2008) found that this model overestimates the ET over a vineyard in an arid desert region with a mean absolute error (MAE) of about 0.057 mm/h. On the contrary, some studies showed that the SW model underestimated half-hourly ET. Zhu et al. (2014) indicated that the SW model tended to underestimate the half-hourly ET with a RMSE value of 0.12 mm/h and a maximum nearly equal to 0.88 mm/h over the spring maize in the arid desert oasis. Also, Ortega-Farias et al. (2010) reported that the SW model underestimated on half-hourly time intervals compared to the EC-measured ET over a drip-irrigated Merlot vineyard in a Mediterranean semi-arid region during the growing season in 2006/2007 with a RMSE equal to 0.046 mm/h and a maximum nearly equal to 0.59 mm/h. Therefore, the performance of the SW model seemed to be variable for different crops and places. Furthermore, several parameters used in the model are set to constant values throughout the study period without considering the seasonal changes. This may impact the quality of the ET predictions, in particular for the physiology-related parameters. In addition, Hu et al. (2009) and Zhu et al. (2013) reported that for long-term simulations of ET, a systematic overestimation or underestimation may occur when constant parameters are used during different vegetation and environmental conditions. The simulated values chosen to retrieve the soil and vegetation resistances were selected based on the good simulation of ET by the SW model when the gap between simulated and measured ET is less than 2 W/m^2.

Local evaluation of the proposed approach

Figure 6 displays the relationship between the retrieved resistances (r_s^s andr_s^v) and the stress indexes (SI_{ss} andSI_{sv}), respectively. The values have been chosen between 12 and 15 h which correspond to the maximum of radiation. The resistance variation ranges (0–3000 s/m for r_s^s and 0–250 s/m for r_s^v) presented in Fig. 6 are in good agreement with those obtained in the literature (Ortega-Farias et al. 2010; Zhu et al. 2014; Zhao et al. 2015). In addition, the obtained trend is similar to that found by Ortega-Farias et al. (2010), Brenner and Incoll (1997) and Zhao et al. (2015) between the soil resistance and the soil humidity which is replaced in this work by the stress indexes. Note, that the stress indexes represent dry conditions when they tend towards 1 and wet conditions when they are close to 0. Figure 6a presents some

Journal : Large 271 | Article No : 701 | Pages : 17 | MS Code : 701 | Dispatch : 30-9-2020

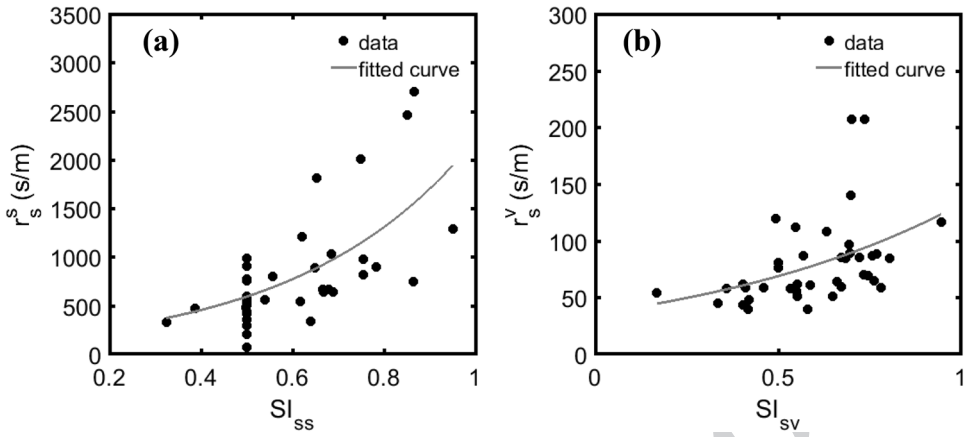

Fig. 6 Relationships between the soil (**a**) and vegetation (**b**) resistances ($r_s^s and r_s^v$) and two stress indexes (SI_{ss}, SI_{sv}) derived from Eqs. 22, 23 for the values between 12 and 15 h. The best fit was also presented (solid line)

soil resistance corresponding to the same stress index value ($SI_{ss} = 0.5$). These (LST, *fc*) points were situated in the transpiration-control zone (see Appendix 2). In this zone T_s was calculated as the average of their endmembers (Eq. 27). The stress index was calculated as the ratio of the difference between T_s and Ts_{min} and the difference between Ts_{max} andTs_{min}. Consequently, the stress index will be continually equal to 0.5 in this zone. This problem was not seen in Fig. 6b for the vegetation resistance since there are few (LST, *fc*) points located in the evaporative control zone. The figure shows the best fits obtained between the soil and the canopy resistances and the stress indexes which are given by:

$$r_s^s = a e^{b \times SI_{ss}},\ R = 0,6 \quad (22)$$

$$r_s^v = c e^{(d \times SI_{sv})},\ R = 0,5 \quad (23)$$

Where the calibration parameters a, c, b and d are equal to 160.25 and 36.02 s/m, 2.62 and 1.30, respectively. Note that the values of these parameters are expected to depend on the canopy, on the local meteorological conditions and on the soil types. Exponential fitting was chosen after testing numerous fitting types given its good representativity of the points scatter.

For the validation of the proposed approach based on optical (NDVI) and thermal (LST) data to compute soil and vegetation resistances in SW model, a comparison between the predicted (average of 0.37 mm/h) and measured (average of 0.34 mm/h) ET at the station scale was illustrated in Fig. 7. The obtained linear regression between simulated and in situ ET is very encouraging with a slope and an intercept of about 0.8 and 0.1 mm/h, respectively. The results are acceptable with a relative RMSE, bias and a R^2 of about 0.29, −0.03 mm/h and 0.48, respectively. The discrepancies in the estimation of ET can be related to the error in the LST estimations and in its partitioning. The statistical performances obtained were in concordance with other

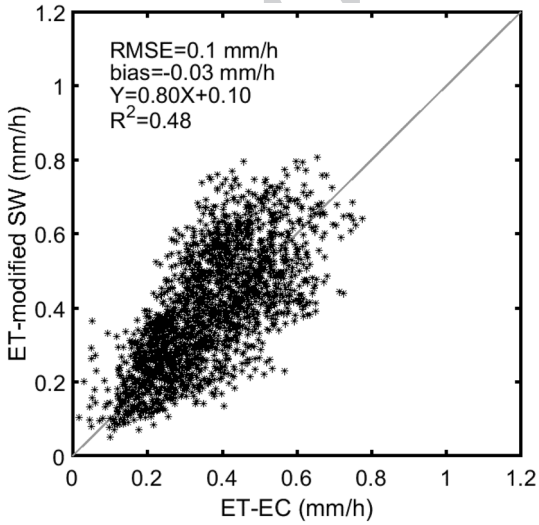

Fig. 7 Half-hourly comparison between estimated ET using the proposed approach and measured one by the Eddy covariance system from January to June 2017

studies that used the thermal proxy based on LST such as (i) FAO-2Kc model used by Olivera-Guerra et al. (2018), who found a RMSE of 0.08 mm/h and R^2 of 0.75 over a wheat plot using daily average values, (ii) Penman–Monteith equation used by Amazirh et al. (2017) who found a RMSE of about 0.12 mm/h and a R^2 of 0.53 over a wheat plot, and (iii) TSEB model where Diarra et al. (2017) obtained a RMSE of 0.10 mm/h and a R^2 of 0.67 over a sugar beet field and a RMSE of 0.11 mm/h and R^2 of 0.42 over a wheat field.

Spatial evaluation of the proposed approach

Stress indexes and resistances spatialization

The SW model has been used to spatialize the evapotranspiration over the piedmont zone. The inputs used in the calculation of the soil and vegetation resistances are difficult to be

Journal : Large 271 | Article No : 701 | Pages : 17 | MS Code : 701 | Dispatch : 30-9-2020

spatialized given the need for soil moisture (SM) maps with high spatial resolution. Indeed, global soil moisture products are generally derived from passive microwave radiometers with a spatial resolution exceeding 10 km, largely too coarse for hydrological applications or from the active one which can provide soil moisture products with high spatial resolution but using complexed method. By contrast, optical and thermal remote sensing data are available with high spatial resolution. Consequently, to overcome this issue the Landsat data have been used instead of the SM to calculate the soil and vegetation resistances using the new proposed approach. Figure 8 presents the spatial variation of the two stress indexes (SI_{ss} and SI_{sv}) at two dates in winter (2017-01-16) and summer (2017-06-09) periods. The stress indexes range between 0 (no stress) and 1 (severe stress) depending on the hydric state of the surface. For both dates, the two indexes exhibited as expected values close to 1 at the river level since there were no growing plants. By contrast, the areas covered by vegetation are characterized by values of SI lower than 1. Both stress indexes achieved high values in summer (date 2017-06-09) exceeding 0.6 which can be justified by the absence of water supply. This is compatible with the available water since the irrigation system is based on surface water that occurs as a result of melting snow. Figure 9 represents the corresponding soil and vegetation resistances, computed from two stress indexes through

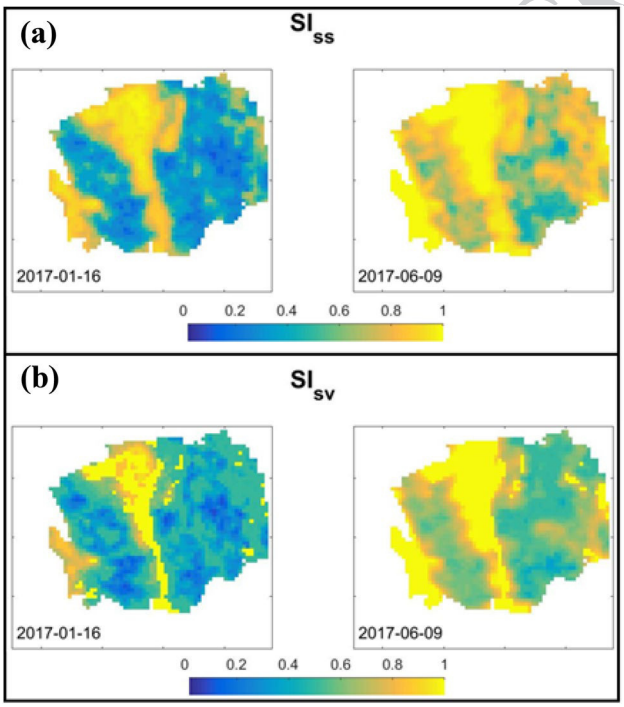

Fig. 8 Maps of the soil (SI_{ss}) and vegetation (SI_{sv}) stress index over the study area for two contrasted dates (2017-01-16) and (2017-06-09)

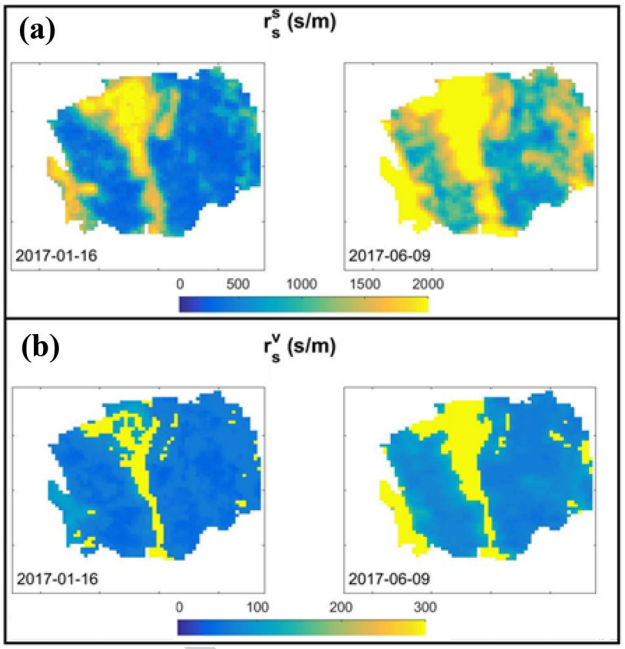

Fig. 9 Maps of the soil (r_s^s) and vegetation (r_s^v) resistance over the study area for two dates (2017-01-16) and (2017-06-09)

two relationships proposed above (Eqs. 22, 23). Vegetation resistance is obviously very high along the river bed since the LAI tends to zero and leads to negligible transpiration. Soil resistance reflects the temporal and spatial variation of the surface soil moisture on the study area. High soil resistance values lead to a sharp decrease in evaporation which is produced by the increase in solar radiation reaching the surface and the low irrigation supply.

Evapotranspiration mapping

Figure 10 displays the spatial and temporal distributions of ET from winter to summer of 2017. For that, 17 Landsat images have been used but only 9 images acquired by Landsat-7 are plotted for illustrating purpose. The spatial distribution of ET is tightly linked to the spatial variation of the fraction cover (Fig. 11), with low values along the river bed which represents a bare soil surface and higher overall the study site which contains a diversity of croplands and arboriculture especially olive trees. The use of an averaged *fc* value integrating different heterogeneous crops which are located within one Landsat pixel can generate some uncertainties in the ET estimates. Indeed, the transpiration for each type of crops is different and depends on its response to the stress conditions due to the difference of LAI and rooting depth. In practice, values of LAI should be calculated for each crop within one Landsat pixel and afterwards a specific formula should be used for deriving the correspondent *fc* of each LAI value. However, this solution cannot be applied in

Journal : Large 271 | Article No : 701 | Pages : 17 | MS Code : 701 | Dispatch : 30-9-2020

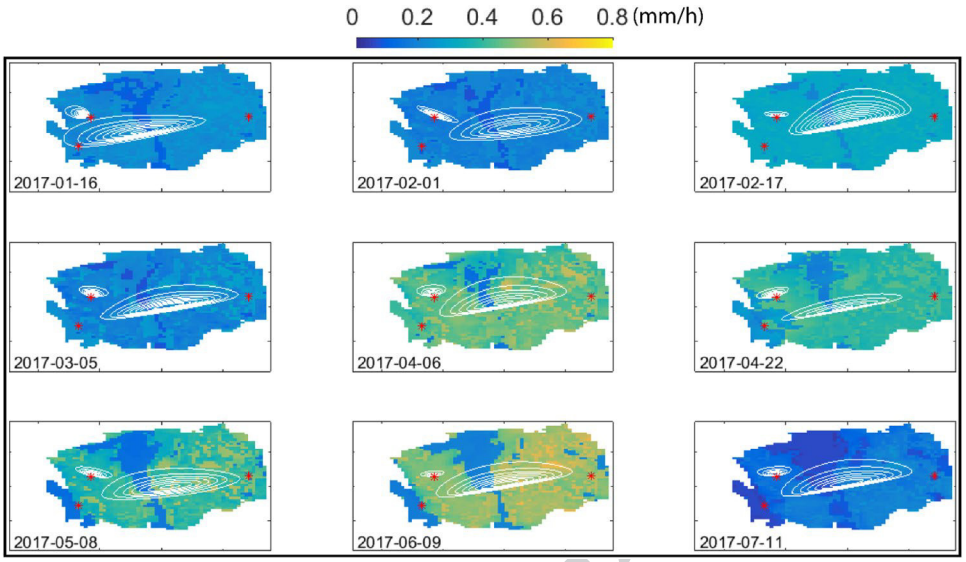

Fig. 10 Evapotranspiration (mm/h) maps over the study area for the dates of the Landsat-7 overpass. The footprint of LAS and EC for the time of the satellite overpass is also represented

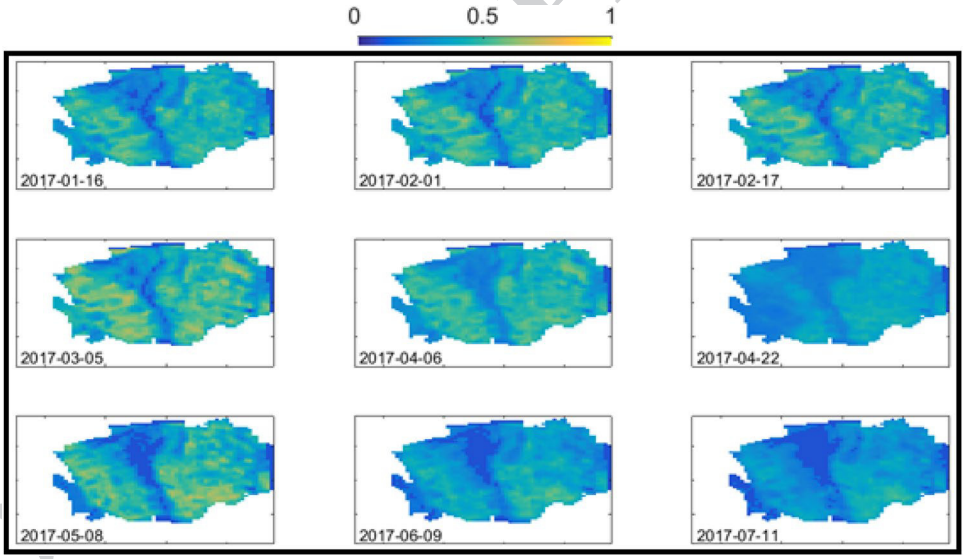

Fig. 11 Fraction cover maps over the study area for the dates that coincide with the overpass of Landsat-7

this study due to the complexity of the site. Therefore, it can be concluded that although great progress has been made in the development of the satellites particularly in terms of spatial resolution, the heterogeneity of our site is one of the major challenges that must be overcome to use the satellite data to assess evapotranspiration in that orchards. Another issue that can generate some uncertainties in the ET estimates over our site was the difficulties of measuring T_v. In fact, measured T_v used in this study was a value attributed to the whole vegetation which means that the same resistance value was attributed to the different crops. In practice, it is difficult to have an adequate place to install the Infra-Red radiometer sensor for providing measurements that can be representative of the whole vegetation in such complex area. To avoid this problem, we need to install an Infra-Red radiometer over each crop which is not feasible as explained for *fc* issue. Otherwise, the estimated T_v using the energy balance model and the hourglass method represents the whole vegetation, meaning that no separation between crops was considered. Consequently, to improve the transpiration estimates using the proposed model, as mentioned before, a high spatial resolution of satellite data is required over such complexity to distinguish between different types of crops. Figure 10 shows also a significant seasonal variation of ET values ranging from less than 200 to up to 520 W/m^2. This variation is mainly related to the available energy and the fraction cover which increase progressively in time from winter to early summer when wheat is harvested (Figs. 11, 12). However, in the fifth day of March, ET values were low even while the available energy was significant (an average

Journal : Large 271 | Article No : 701 | Pages : 17 | MS Code : 701 | Dispatch : 30-9-2020

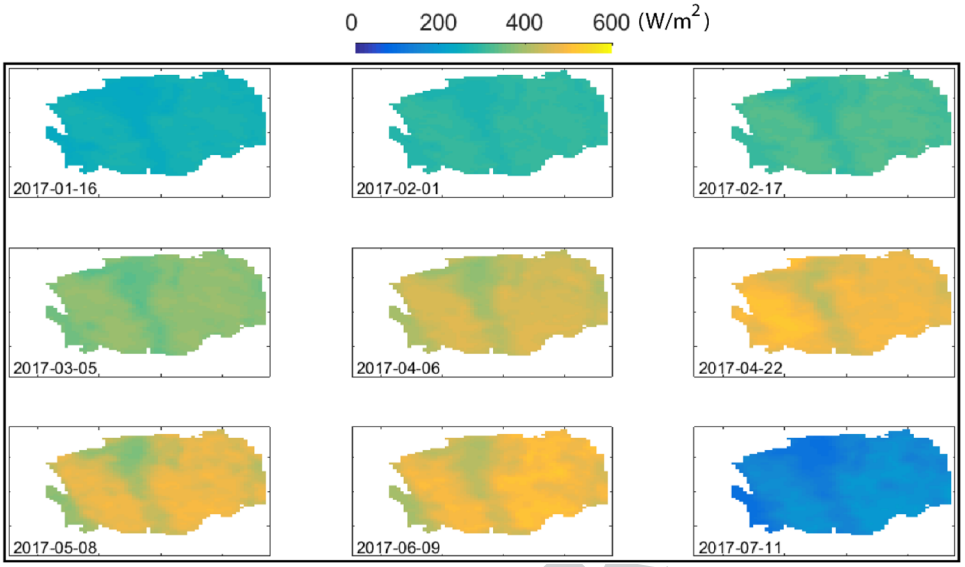

Fig. 12 Available energy (W/m^2) maps over the study area for the dates that coincide with the overpass of Landsat-7

of about 420 W/m^2) and the fraction cover was high (an average of about 0.65). This is attributed to the atmospheric saturation, as the air temperature was low (about 14 °C) and the air humidity was high (71.45%). This drastically decreased the amount of the evaporative demand.

The footprints of the scintillometer and EC were also presented in Fig. 10 to show the variation of the source area of the LAS and EC measurements. The footprint was used to weight the ET values from the maps at the time of the satellites overpass. The modeled ET values were validated by comparing them to the measurements (over the LAS and EC footprints). Figure 13 shows good consistency between the simulated ET values, using SW model driven by Landsat 7 and 8 and observed one. The statistical analysis between the model and the LAS measurements showed better agreement than those obtained between the model and the EC measurements with an RMSE and R^2 of about 0.08 mm/h and 0.80, respectively, for the LAS and 0.1 mm/h and 0.47, respectively, for the EC. This can be justified by the accuracy of the relation between the resistances and the stress indexes which could be stronger over other plots than the plot where the calibration was done. Otherwise, the comparison with EC and LAS measurements show an underestimation with a slope of about 0.84 and 0.88 for LAS and EC, respectively. This underestimation of the ET by the model is probably justified by the error on the satellites LST. The processing of this data as mentioned in Sect. (Remote sensing data) can cause a surface temperature overestimation. This will generate an overestimation of the resistances and consequently, the ET will be underestimated. Additionally, in our model, for an NDVI less than 0.2 the LAI is set to 0 while, some sparse vegetation can grow along the river which is not enough to exceed the NDVI threshold. This can provide low estimated ET. The results obtained are relevant compared to other studies that used the scintillometry method to evaluate the performance of the different model

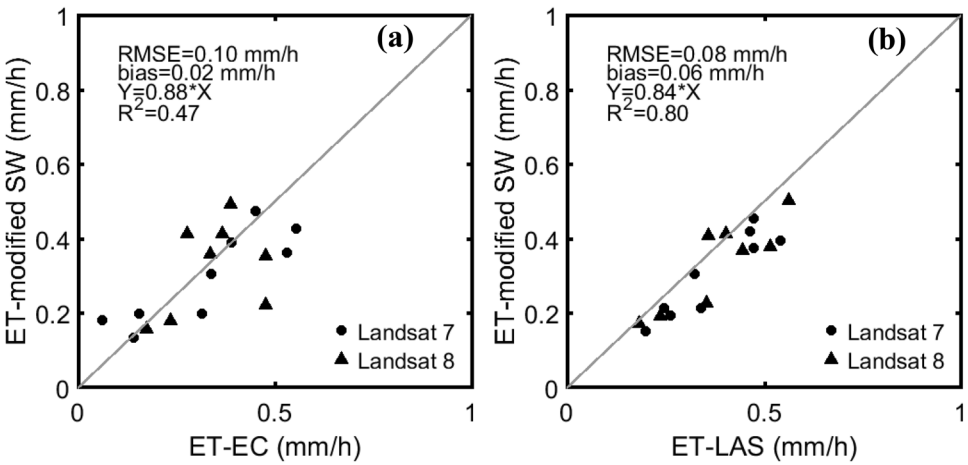

Fig. 13 Comparison of estimated evapotranspiration from the modified SW model driven by Landsat-7 and Landsat-8 and measured by the eddy covariance system (**a**) and the scintillometer (**b**)

Journal : Large 271 | Article No : 701 | Pages : 17 | MS Code : 701 | Dispatch : 30-9-2020

in estimating ET. Ait Hssaine et al. (2018) have found an RMSE and R^2 of about 0.11 mm/h and 0.52, respectively, between scintillometer measurement and ET estimated using the Two-source Energy Balance model (TSEB) over an heterogeneous area covered by Millet (58%), Fallow savannah (23%) and Degraded shrubs (19%) in the region of Niamey city, Niger. In the same vein, Saadi et al. (2018) have used an extra-large scintillometer to validate ET values estimated using Soil Plant Atmosphere and Remote Sensing Evapotranspiration (SPARSE) model over a landscape dominated by agriculture products (cereals, olive groves, fruit trees, market gardening). They found a RMSE and R^2 of about 0.06 mm/h and 0.55, respectively.

The proposed approach has some limitations compared to traditional models such as SEBAL or METRIC. In fact, these models don't need an accurate surface temperature which demands complicated treatments and corrections (Allen et al. 2007; Gonzalez-Dugo et al. 2009) or air temperature measurements. In contrary, our approach requires accurate values of surface temperature to correctly estimate the different resistances. Otherwise, Choi et al. (2009) reported that METRIC forces the predicted flux distributions to scale between wet and dry hydrologic conditions, which may not necessarily be present in every image. In contrast, the proposed approach does not make this assumption and depend only on moisture variability represented by the stress indexes in the model. In addition, the proposed approach is a two-source model which allows to the ET partitioning into soil evaporation (E) and plant transpiration (T). This is an important advantage that provides precise information about the real amount of water needs by crops. However, in this study, the partition of the soil evaporation and the transpiration was not evaluated given the unavailability of the measurement devices of separate E/T in the study area. The proposed approach was calibrated over olive tree with an understory of annual crops. The established relation between the stress indexes and the resistances (Eqs. 22, 23) over this type of cover may need to be adapted over other vegetation types which their sensitivity to the stress conditions is different. Otherwise, although the study site presents a high heterogeneity of vegetation type, the proposed approach shows good consistency when the simulation values were compared to the LAS measurements. Overall, this modification of the SW model is needed to be tested with other data set and over other meteorological conditions to evaluate its robustness and improve the relation found between the resistances and the thermal stress indexes.

The proposed approach has a great potential for estimating ET over complex surface. This provides a precise information about the real amount of crops water needs for improving large scale sustainable irrigation strategy. In addition, the use of thermal/optical remote sensing data has proven to be remarkably accurate and robust for estimating the ET over complex and heterogeneous area. However, testing this approach with other data set and over other meteorological conditions to evaluate its robustness and improve the relation found between the resistances and the thermal stress indexes is necessary. Likewise applying other constraint on soil evaporation and plant transpiration as the soil moisture derived from the microwave data will be of great importance to improve the soil and vegetation resistances estimates.

Conclusion

Accurate and consistent estimation of evapotranspiration is essential in determining the crop water requirement. The aim of this work was to map the ET over a heterogeneous surface in the piedmont of Atlas mountain using the SW model.

The spatialization of this model requires knowledge of the spatial variation of certain inputs such as the soil moisture which is not easy to be obtained with high spatial resolution taking into account the heterogeneity of the site. The idea that has been proposed is to use the thermal and optical data provided from Landsat 7 and 8 instead to soil moisture which is difficult to obtain. Soil and vegetation resistances (r_s^s, r_s^v) were linked to the stress indexes which are computed from a normalization of vegetation and soil temperature by their endmembers. The vegetation and soil temperatures are derived using the Hourglass method forced by vegetation fraction and meteorological data. The endmembers of the two surface temperature components are simulated using a surface energy balance model. The following conclusions were drawn from the results of the study:

First, SW model was tested locally and acceptable results were obtained in estimating ET with a relative RMSE and bias are equal to 0.38 and −0.1 mm/h, respectively.

Second, the resistances values were inverted from the SW model and used to found the empirical relations based on the stress indexes. The method was validated at local scale by comparing the results with EC system and the statistical performance were encouraging with a relative RMSE and bias equal to 0.29 and −0.03 mm/h, respectively.

Finally, the proposed approach was spatialized using Landsat 7 and 8 data and confirmed its accuracy by comparison to the LAS and EC measurements. The RMSE, bias and R^2 are equal to 0.08 mm/h, 0.06 mm/h and 0.80, respectively, compared to the LAS and equal to 0.1 mm/h, 0.02 mm/h and 0.47, respectively, compared to the EC.

This approach proves the utility of thermal and optical remote sensing for estimating accurate ET at a regional scale. This will be even better if these data were provided with a high revisit time keeping the same spatial resolution. Such improvement is possible with the advent of the TRISHNA mission as reported by Lagouarde and Bhattacharya (2018). In addition to optical and thermal data

Journal : Large 271 | Article No : 701 | Pages : 17 | MS Code : 701 | Dispatch : 30-9-2020

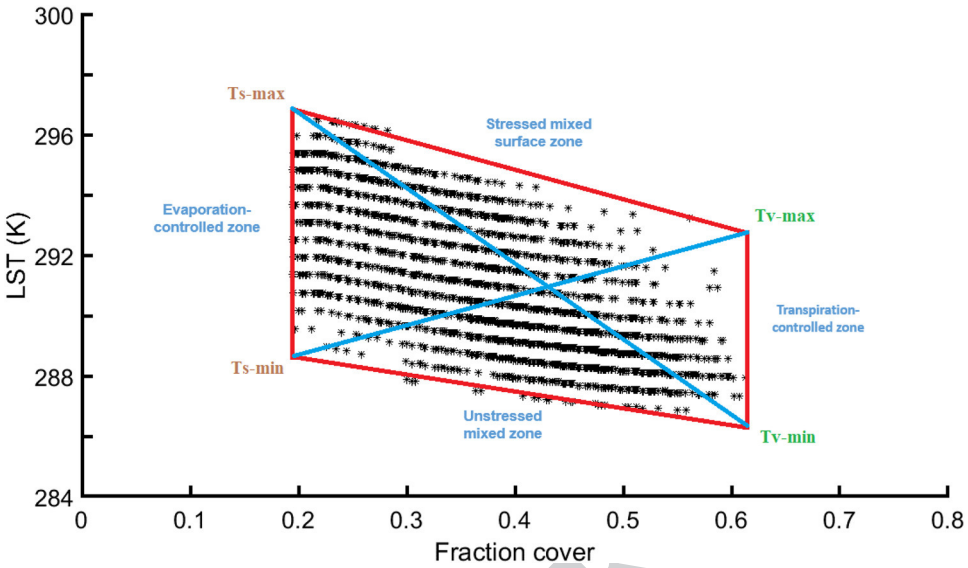

Fig. 14 Illustration of a polygon defined in the land surface temperature-fractional vegetation cover space contains four distinct zones (Evaporation-controlled zone, stressed mixed surface zone, transpiration-controlled zone and unstressed mixed zone

other relevant remote sensing product could be used to feed the proposed approach. In particular, the microwave data, which are strongly related to the soil hydric status, can provide a promising issue to improve irrigation management. Finally, it should be noted that the procedure proposed here has been solely tested during one growing season. Further tests of this procedure with other data sets and over other surface conditions are needed.

Acknowledgments This work was carried out within the frame of the Joint International Laboratory TREMA (https://lmi-trema.ma). Setup was funded by CNRST SAGESSE project and German Cooperation Giz within the frame of the Hydraulic Basin Agency of the Tensift (ABHT). PHC TBK/18/61 project is acknowledged for providing Jamal Elfarkh a travel grant. The authors wish to thank the projects: RISE-H2020-ACCWA (grant agreement no: 823965) and ERANET-MED03-62 CHAAMS for partly funding the experiments.

Appendix 1

The LAS measurement is the average of an entire area where each part of it contributes with a percentage depends on its position, weight and wind speed. To obtain this contribution several analytical and Lagrangian models of footprint have been developed (Schuepp et al. 1990; Horst and Weil 1992; Rannik et al. 2000). In this work, we used the model of Horst and Weil (1992) that relates the flux measured at z_m to the surface distribution of the flux: where f is the footprint function relates the flux measured at z_m, $F(x, y, z_m)$ to the spatial distribution of surface fluxes, $F(x, y, z = 0) = F_0(x, y)$. x and y are the downwind and crosswind distances (m) from the point where the measurements are taken, respectively.

$$F(x, y, z_m) = \int_{-\infty}^{\infty} \int_{\infty}^{x} F_0(x', y') f(x - x', y - y', z_m) \mathrm{d}x' \mathrm{d}y' \tag{24}$$

As already mentioned, each point is weighted according to the spatial weighting function of the LAS (Meijninger 2003): Where $F_{\mathrm{LAS}}(x, y, Z_{\mathrm{LAS}})$ is the LAS footprint, and $F(x, y, Z_{\mathrm{LAS}})$ is the flux footprint for a point located at d distance from the transmitter. $G(d)$ is the scintillometer path-weighting function for the position located at d distance.

$$F_{\mathrm{LAS}}(x, y, Z_{\mathrm{LAS}}) = \sum_{i=1}^{N} F(x, y, Z_{\mathrm{LAS}}) G(d) \tag{25}$$

Appendix 2

The partitioning of LST into its soil and vegetation components is based on the LST and *fc* within the polygon (Fig. 14) to determine one of the temperature components T_{v} or T_{s} as follow:

For a given data point located in the evaporation-controlled zone, T_{v} computed as:

$$T_{\mathrm{v}} = \frac{T\mathrm{v}_{\max} + T\mathrm{v}_{\min}}{2} \tag{26}$$

For a given data point located in the transpiration-controlled zone, T_{s} computed as:

$$T_{\mathrm{s}} = \frac{T\mathrm{s}_{\max} + T\mathrm{s}_{\min}}{2} \tag{27}$$

For a given data point located in the stressed mixed surface zone, T_v computed as:

$$T = \frac{\mathrm{LST} - T\mathrm{s}_{\max}}{fc} + T\mathrm{s}_{\max} \quad (28)$$

$$T_v = \frac{T\mathrm{v}_{\max} + T}{2} \quad (29)$$

For a given data point located in the unstressed mixed zone, T_v computed as:

$$T = \frac{\mathrm{LST} - T\mathrm{s}_{\min}}{fc} + T\mathrm{s}_{\min} \quad (30)$$

$$T_v = \frac{T\mathrm{v}_{\max} + T}{2} \quad (31)$$

Then, the other component T_v or T_s was derived based on a linear decomposition of the LST in its vegetation and soil components as follows:

$$\mathrm{LST} = \left((1-fc)T_s^4 + fcT_v^4\right)^{1/4} \quad (32)$$

In what follows, fc is derived from Landsat NDVI using the following equation:

$$fc = 1 - \mathrm{e}^{-0.5 \times \mathrm{LAI}}. \quad (33)$$

References

Ait Hssaine BA, Ezzahar J, Jarlan L et al (2018) Combining a two source energy balance model driven by MODIS and MSG-SEVIRI products with an aggregation approach to estimate turbulent fluxes over sparse and heterogeneous vegetation in Sahel region (Niger). Remote Sens 10(6):974. https://doi.org/10.3390/rs10060974

Albergel C (2010) Assimilation de données de télédétection dans le modèle ISBA-A-gs pour une analyse conjointe de la biomasse et de l'état hydrique du sol. https://www.theses.fr

Allen RG, Pereira LS, Howell TA, Jensen ME (2011) Evapotranspiration information reporting: I. factors governing measurement accuracy. Agric Water Manag 98:899–920. https://doi.org/10.1016/j.agwat.2010.12.015

Allen RG, Tasumi M, Morse A et al (2007) Journal of irrigation and drainage engineering satellite-based energy balance for Mapping Evapotranspiration with Internalized Calibration (METRIC)—applications. J Irrig Drain Eng. https://doi.org/10.1061/(ASCE)0733-9437(2007)133

Allen RG, Tasumi M, Morse A, Trezza R (2005) A landsat-based energy balance and evapotranspiration model in Western US water rights regulation and planning. Irrig Drain Syst 19:251–268. https://doi.org/10.1007/s10795-005-5187-z

Amazirh A, Er-Raki S, Chehbouni A et al (2017) Modified Penman-Monteith equation for monitoring evapotranspiration of wheat crop: Relationship between the surface resistance and remotely sensed stress index. Biosyst Eng 164:68–84. https://doi.org/10.1016/j.biosystemseng.2017.09.015

Amazirh A, Merlin O, Er-Raki S et al (2018) Retrieving surface soil moisture at high spatio-temporal resolution from a synergy between Sentinel-1 radar and Landsat thermal data: a study case over bare soil. Remote Sens Environ 211:321–337

Aouade G, Ezzahar J, Amenzou N et al (2016) Combining stable isotopes and micrometeorological measurements for partitioning evapotranspiration of winter wheat into soil evaporation and plant transpiration in a semi-arid region. Agric Water Manag 177(1):181–192. https://doi.org/10.1016/j.agwat.2016.07.021

Aouade G, Jarlan L, Ezzahar J et al (2020) Evapotranspiration partition using the multiple energy balance version of the ISBA-A-gs land surface model over two irrigated crops in a semi-arid Mediterranean region (Marrakech, Morocco). Hydrol Earth Syst Sci Discuss 24(7):3789–3814. https://doi.org/10.5194/hess-24-3789-2020

Bastiaanssen WGM, Pelgrum H, Wang J et al (1998) A remote sensing surface energy balance algorithm for land (SEBAL): 2. Validation J Hydrol. https://doi.org/10.1016/S0022-1694(98)00254-6

Bhattarai N, Mallick K, Stuart J et al (2019) An automated multi-model evapotranspiration mapping framework using remotely sensed and reanalysis data. Remote Sens Environ 229:69–92. https://doi.org/10.1016/j.rse.2019.04.026

Blinda M (2012) Cahier 14 EAU EFFICIENCE Vers une meilleure efficience de l'utilisation de l'eau en Méditerranée

Boulet G, Mougenot B, Lhomme, et al (2015) The SPARSE model for the prediction of water stress and evapotranspiration components from thermal infra-red data and its evaluation over irrigated and rainfed wheat. Hydrol Earth Syst Sci 19(11):4653–4672. https://doi.org/10.5194/hess-19-4653-2015

Bouimouass H, Fakir Y, Tweed S, Leblanc M (2020) Groundwater recharge sources in semiarid irrigated mountain fronts. Hydrol Process 34:1598–1615. https://doi.org/10.1002/hyp.13685

Braud I, Dantas-Antonino AC, Vauclin M et al (1995) A simple soil-plant-atmosphere transfer model (SiSPAT) development and field verification. J Hydrol 166:213–250. https://doi.org/10.1016/0022-1694(94)05085-C

Brenner AJ, Incoll LD (1997) The effect of clumping and stomatal response on evaporation from sparsely vegetated shrublands. Agric For Meteorol 84:187–205. https://doi.org/10.1016/S0168-1923(96)02368-4

Carlson TN, Capehart WJ, Gillies RR (1995) A new look at the simplified method for remote sensing of daily evapotranspiration. Remote Sens Environ 54:161–167. https://doi.org/10.1016/0034-4257(95)00139-R

Choi M, Kustas WP, Anderson MC et al (2009) An intercomparison of three remote sensing-based surface energy balance algorithms over a corn and soybean production region (Iowa, U.S.) during SMACEX. Agric For Meteorol 149:2082–2097. https://doi.org/10.1016/j.agrformet.2009.07.002

Diarra A, Jarlan L, Er-Raki S et al (2017) Performance of the two-source energy budget (TSEB) model for the monitoring of evapotranspiration over irrigated annual crops in North Africa. Agric Water Manag 193:71–88. https://doi.org/10.1016/j.agwat.2017.08.007

Duchemin B, Hagolle O, Mougenot B et al (2008) Agrometerological study of semi-ard areas: an experiment for analysing the potential of time series of FORMOSAT-2 images (Tensift-Marrakech plain). Int J Remote Sens 29:5291–5300. https://doi.org/10.1080/01431160802036482

Er-Raki S, Chehbouni A, Boulet G, Williams DG (2010a) Using the dual approach of FAO-56 for partitioning ET into soil and plant components for olive orchards in a semi-arid region. Agric Water Manag 97:1769–1778. https://doi.org/10.1016/j.agwat.2010.06.009

Er-Raki S, Chehbouni A, Duchemin B (2010b) Combining satellite remote sensing data with the FAO-56 dual approach for water use

mapping in irrigated wheat fields of a semi-arid region. Remote Sens. https://doi.org/10.3390/rs2010375
Ezzahar J, Chehbouni A (2009) The use of scintillometry for validating aggregation schemes over heterogeneous grids. Agric For Meteorol 149:2098–2109. https://doi.org/10.1016/j.agrformet.2009.09.004
Ezzahar J, Chehbouni A, Er-Raki S, Hanich L (2009a) Combining a large aperture scintillometer and estimates of available energy to derive evapotranspiration over several agricultural fields in a semi-arid region. Plant Biosyst 143:209–221. https://doi.org/10.1080/11263500802710036
Ezzahar J, Chehbouni A, Hoedjes J et al (2009b) Combining scintillometer measurements and an aggregation scheme to estimate area-averaged latent heat flux during the AMMA experiment. J Hydrol 375:217–226. https://doi.org/10.1016/j.jhydrol.2009.01.010
Ezzahar J, Chehbouni A, Hoedjes JCB et al (2007) The use of the scintillation technique for monitoring seasonal water consumption of olive orchards in a semi-arid region. Agric Water Manag 89:173–184. https://doi.org/10.1016/j.agwat.2006.12.015
Fang B, Lei H, Zhang Y et al (2020) Spatio-temporal patterns of evapotranspiration based on upscaling eddy covariance measurements in the dryland of the North China Plain. Agric For Meteorol. https://doi.org/10.1016/j.agrformet.2019.107844
Gentine P, Entekhabi D, Chehbouni A et al (2007) Analysis of evaporative fraction diurnal behaviour. Agric For Meteorol 143:13–29. https://doi.org/10.1016/j.agrformet.2006.11.002
Gohar AA, Cashman A, Ward FA (2019) Managing food and water security in small island states: new evidence from economic modelling of climate stressed groundwater resources. J Hydrol 569:239–251. https://doi.org/10.1016/j.jhydrol.2018.12.008
Gonzalez-Dugo MP, Neale CMU, Mateos L et al (2009) A comparison of operational remote sensing-based models for estimating crop evapotranspiration. Agric For Meteorol 149:1843–1853. https://doi.org/10.1016/j.agrformet.2009.06.012
Green S, Clothier B, Jardine B (2003) Theory and Practical Application of Heat Pulse to Measure Sap Flow. In: Agronomy Journal. pp 1371–1379
Guswa AJ, Celia MA, Rodriguez-Iturbe I (2002) Models of soil moisture dynamics in ecohydrology: a comparative study. Water Resour Res 38:5-1-5–15. https://doi.org/10.1029/2001wr000826
Harris PP, Huntingford C, Cox PM et al (2004) Effect of soil moisture on canopy conductance of Amazonian rainforest. Agric For Meteorol 122:215–227. https://doi.org/10.1016/j.agrformet.2003.09.006
Horst TW, Weil JC (1994) How far is far enough? The fetch requirements for micrometeorological measurement of surface fluxes. J Atmos Ocean Technol 11:1018–1025. https://doi.org/10.1175/1520-0426(1994)011<1018:hfifet>2.0.co;2
Horst TW, Weil JC (1992) Footprint estimation for scalar flux measurements in the atmospheric surface layer. Boundary-Layer Meteorol 59:279–296. https://doi.org/10.1007/BF00119817
Hu Z, Yu G, Zhou Y et al (2009) Partitioning of evapotranspiration and its controls in four grassland ecosystems: Application of a two-source model. Agric For Meteorol 149:1410–1420. https://doi.org/10.1016/j.agrformet.2009.03.014
Huang G, Li X, Huang C et al (2016) Representativeness errors of point-scale ground-based solar radiation measurements in the validation of remote sensing products. Remote Sens Environ 181:198–206. https://doi.org/10.1016/j.rse.2016.04.001
Jackson RD, Reginato RJ, Idso SB (1977) Wheat canopy temperature: a practical tool for evaluating water requirements. Water Resour Res 13:651–656. https://doi.org/10.1029/WR013i003p00651
Liu SM, Xu ZW, Wang WZ, Jia ZZ, Zhu MJ, Bai J, Wang JM (2011) A comparison of eddy-covariance and large aperture scintillometer measurements with respect to the energy balance closure problem. Hydrol Earth Syst Sci 15:1291–1306
Mauder M, Liebethal C, Göckede M, Leps JP, Beyrich F, Foken T (2006) Processing and quality control of flux data during LITFASS-2003. Bound Layer Meteorol 121:67–88
Meijninger WML (2003) Surface fluxes over natural landscapes using scintillometry
Merlin O (2013) An original interpretation of the wet edge of the surface temperature-albedo space to estimate crop evapotranspiration (SEB-1S), and its validation over an irrigated area in northwestern Mexico. Hydrol Earth Syst Sci 17:3623–3637. https://doi.org/10.5194/hess-17-3623-2013
Merlin O, Rüdiger C, Al Bitar A et al (2012) Disaggregation of SMOS soil moisture in Southeastern Australia. IEEE Trans Geosci Remote Sens 50:1556–1571. https://doi.org/10.1109/TGRS.2011.2175000
Merlin O, Stefan VG, Amazirh A et al (2016) Modeling soil evaporation efficiency in a range of soil and atmospheric conditions using a meta-analysis approach. Water Resour Res 52:3663–3684. https://doi.org/10.1002/2015WR018233
Moran MS, Clarke TR, Inoue Y, Vidal A (1994) Estimating crop water deficit using the relation between surface-air temperature and spectral vegetation index. Remote Sens Environ 49:246–263. https://doi.org/10.1016/0034-4257(94)90020-5
Neale CMU, Jayanthi H, Wright JL (2005) Irrigation water management using high resolution airborne remote sensing. Irrig Drain Syst 19:321–336. https://doi.org/10.1007/s10795-005-5195-z
Noilhan J, Mahfouf JF (1996) The ISBA land surface parameterisation scheme. Glob Planet Change 13:145–159. https://doi.org/10.1016/0921-8181(95)00043-7
Norman JM, Kustas WP, Humes KS (1995) Source approach for estimating soil and vegetation energy fluxes in observations of directional radiometric surface temperature. Agric For Meteorol 77:263–293. https://doi.org/10.1016/0168-1923(95)02265-Y
Olivera-Guerra L, Merlin O, Er-Raki S et al (2018) Estimating the water budget components of irrigated crops: combining the FAO-56 dual crop coefficient with surface temperature and vegetation index data. Agric Water Manag 208:120–131. https://doi.org/10.1016/j.agwat.2018.06.014
Olivera-Guerra L, Merlin O, Er-Raki S (2020) Irrigation retrieval from Landsat optical/thermal data integrated into a crop water balance model: a case study over winter wheat fields in a semi-arid region. Remote Sens Environ. https://doi.org/10.1016/j.rse.2019.111627
Ortega-Farias S, Carrasco M, Olioso A et al (2007) Latent heat flux over Cabernet Sauvignon vineyard using the Shuttleworth and Wallace model. Irrig Sci 25:161–170. https://doi.org/10.1007/s00271-006-0047-7
Ortega-Farias S, Poblete-Echeverría C, Brisson N (2010) Parameterization of a two-layer model for estimating vineyard evapotranspiration using meteorological measurements. Agric For Meteorol 150:276–286. https://doi.org/10.1016/j.agrformet.2009.11.012
Plattner G-K, Stocker T, Midgley P, Tignor M (2009) INTERGOVERNMENTAL PANEL ON CLIMATE CHANGE IPCC Expert Meeting on the Science of Alternative Metrics Meeting Report Supporting material prepared for consideration by the Intergovernmental Panel on Climate Change. This material has not been subjected to for
Rafi Z, Merlin O, Le Dantec V et al (2019) Partitioning evapotranspiration of a drip-irrigated wheat crop: Inter-comparing eddy covariance-, sap flow-, lysimeter- and FAO-based methods. Agric For Meteorol 265:310–326. https://doi.org/10.1016/j.agrformet.2018.11.031
Ramírez DA, Bellot J, Domingo F, Blasco A (2007) Can water responses in *Stipa tenacissimaL.* during the summer season be promoted by non-rainfall water gains in soil? Plant Soil 291:67–79. https://doi.org/10.1007/s11104-006-9175-3

Rannik U, Aubinet M, Kurbanmuradov O et al (2000) Footprint analysis for measurements over a heterogeneous forest. Boundary-Layer Meteorol 97:137–166. https://doi.org/10.1023/A:1002702810929

Roerink GJ, Su Z, Menenti M (2000) S-SEBI: A simple remote sensing algorithm to estimate the surface energy balance. Phys Chem Earth Part B Hydrol Ocean Atmos 25:147–157. https://doi.org/10.1016/S1464-1909(99)00128-8

Saadi S, Boulet G, Bahir M et al (2018) Assessment of actual evapotranspiration over a semiarid heterogeneous land surface by means of coupled low-resolution remote sensing data with an energy balance model: comparison to extra-large aperture scintillometer measurements. Hydrol Earth Syst Sci 22:2187–2209. https://doi.org/10.5194/hess-22-2187-2018

Samanta S, Mackay DS, Clayton MK et al (2007) Bayesian analysis for uncertainty estimation of a canopy transpiration model. Water Resour Res 43:1–13. https://doi.org/10.1029/2006WR005028

Sánchez JM, López-Urrea R, Valentín F et al (2019) Lysimeter assessment of the simplified two-source energy balance model and eddy covariance system to estimate vineyard evapotranspiration. Agric For Meteorol 274:172–183. https://doi.org/10.1016/j.agrformet.2019.05.006

Schuepp PH, Leclerc MY, MacPherson JI, Desjardins RL (1990) Footprint prediction of scalar fluxes from analytical solutions of the diffusion equation. Boundary-Layer Meteorol 50:355–373. https://doi.org/10.1007/BF00120530

Seguin B, Itier B (1983) Using midday surface temperature to estimate daily evaporation from satellite thermal IR data. Int J Remote Sens 4:371–383. https://doi.org/10.1080/01431168308948554

Semmens KA, Anderson MC, Kustas WP et al (2016) Monitoring daily evapotranspiration over two California vineyards using Landsat 8 in a multi-sensor data fusion approach. Remote Sens Environ 185:155–170. https://doi.org/10.1016/j.rse.2015.10.025

Sene KJ (1994) Parameterisations for energy transfers from a sparse vine crop. Agric For Meteorol 71:1–18. https://doi.org/10.1016/0168-1923(94)90097-3

Shuttleworth WJ, Wallace JS (1985) Evaporation from sparse crops-an energy combination theory. Q J R Meteorol Soc 111:839–855. https://doi.org/10.1002/qj.49711146510

Singh RK, Senay GB, Velpuri NM et al (2014) On the downscaling of actual evapotranspiration maps based on combination of MODIS and landsat-based actual evapotranspiration estimates. Remote Sens 6:10483–10509. https://doi.org/10.3390/rs61110483

Stefan VG, Merlin O, Er-Raki S et al (2015) Consistency between In Situ, model-derived and high-resolution-image-based soil temperature endmembers: Towards a robust data-based model for multi-resolution monitoring of crop evapotranspiration. Remote Sens 7:10444–10479. https://doi.org/10.3390/rs70810444

Steppe K, De Pauw DJW, Doody TM, Teskey RO (2010) A comparison of sap flux density using thermal dissipation, heat pulse velocity and heat field deformation methods. Agric For Meteorol 150:1046–1056. https://doi.org/10.1016/j.agrformet.2010.04.004

Su Z (2002) The Surface Energy Balance System (SEBS) for estimation of turbulent heat fluxes. Hydrol Earth Syst Sci 6:85–100. https://doi.org/10.5194/hess-6-85-2002

Tan S, Wu B, Yan N (2019) A method for downscaling daily evapotranspiration based on 30 m surface resistance. J Hydrol. https://doi.org/10.1016/j.jhydrol.2019.06.054

Tang R, Li ZL (2015) Evaluation of two end-member-based models for regional land surface evapotranspiration estimation from MODIS data. Agric For Meteorol 202:69–82. https://doi.org/10.1016/j.agrformet.2014.12.005

Twine TE, Kustas WP, Norman JM et al (2000) Correcting eddy-covariance flux underestimates over a grassland. Agric For Meteorol 103:279–300. https://doi.org/10.1016/S0168-1923(00)00123-4

Verhoef A, Fernández-Gálvez J, Diaz-Espejo A et al (2006) The diurnal course of soil moisture as measured by various dielectric sensors: effects of soil temperature and the implications for evaporation estimates. J Hydrol 321:147–162. https://doi.org/10.1016/j.jhydrol.2005.07.039

Villagarcía L, Were A, García M, Domingo F (2010) Sensitivity of a clumped model of evapotranspiration to surface resistance parameterisations: application in a semi-arid environment. Agric For Meteorol 150:1065–1078. https://doi.org/10.1016/j.agrformet.2010.04.006

Wang L, Parodi GN, Su Z (2008) SEBS module beam: A practical tool for surface energy balance estimates from remote sensing data. In: European Space Agency, (Special Publication) ESA SP

Ward HC (2017) Scintillometry in urban and complex environments : a review. Meas Sci Technol 28:27. https://doi.org/10.1088/1361-6501/aa5e85

Were A, Villagarcia L, Domingo F et al (2007) Analysis of effective resistance calculation methods and their effect on modelling evapotranspiration in two different patches of vegetation in semi-arid SE Spain. Hydrol Earth Syst Sci 11:1529–1542. https://doi.org/10.5194/hess-11-1529-2007

Wittich KP (1997) Some simple relationships between land-surface emissivity, greenness and the plant cover fraction for use in satellite remote sensing. Int J Biometeorol 41:58–64. https://doi.org/10.1007/s004840050054

Yee MS, Pauwels VRN, Daly E et al (2015) A comparison of optical and microwave scintillometers with eddy covariance derived surface heat fluxes. Agric For Meteorol 213:226–239. https://doi.org/10.1016/j.agrformet.2015.07.004

Zhang B, Kang S, Li F, Zhang L (2008) Comparison of three evapotranspiration models to Bowen ratio-energy balance method for a vineyard in an arid desert region of northwest China. Agric For Meteorol 148:1629–1640. https://doi.org/10.1016/j.agrformet.2008.05.016

Zhang B, Kang S, Zhang L et al (2009) An evapotranspiration model for sparsely vegetated canopies under partial root-zone irrigation. Agric For Meteorol 149:2007–2011. https://doi.org/10.1016/j.agrformet.2009.07.007

Zhao P, Li S, Li F et al (2015) Comparison of dual crop coefficient method and Shuttleworth–Wallace model in evapotranspiration partitioning in a vineyard of northwest China. Agric Water Manag 160:41–56. https://doi.org/10.1016/j.agwat.2015.06.026

Zhu G, Su Y, Li X et al (2013) Estimating actual evapotranspiration from an alpine grassland on Qinghai-Tibetan plateau using a two-source model and parameter uncertainty analysis by Bayesian approach. J Hydrol 476:42–51. https://doi.org/10.1016/j.jhydrol.2012.10.006

Zhu GF, Li X, Su YH et al (2014) Simultaneously assimilating multivariate data sets into the two-source evapotranspiration model by Bayesian approach: application to spring maize in an arid region of northwestern China. Geosci Model Dev 7:1467–1482. https://doi.org/10.5194/gmd-7-1467-2014

Zieliński M, Fortuniak K, Pawlak W, Siedlecki M (2013) Turbulent sensible heat flux in łódź, central poland, obtained from scintillometer and eddy covariance measurements. Meteorol Zeitschrift 22:603–613. https://doi.org/10.1127/0941-2948/2013/0448

Zieliński M, Fortuniak K, Pawlak W, Siedlecki M (2017) Influence of mean rooftop-level estimation method on sensible heat flux retrieved from a large-aperture scintillometer over a city centre. Boundary Layer Meteorol 164:281–301. https://doi.org/10.1007/s10546-017-0254-1

Journal:	**271**
Article:	**701**

Author Query Form

Please ensure you fill out your response to the queries raised below and return this form along with your corrections

Dear Author

During the process of typesetting your article, the following queries have arisen. Please check your typeset proof carefully against the queries listed below and mark the necessary changes either directly on the proof/online grid or in the 'Author's response' area provided below

Query	Details Required	Author's Response
AQ1	Reference: Reference [Tardy et al. (2016)] was mentioned in the manuscript; however, this was not included in the reference list. As a rule, all mentioned references should be present in the reference list. Please provide the reference details to be inserted in the reference list.	
AQ2	Please provide publisher location and editor name for reference [Green et al., 2003].	
AQ3	Please provide journal title, volume number, issue number, page range/DOI for references [Meijninger, 2003].	
AQ4	Please provide full details and complete sentence for references [Plattner et al., 2009].	
AQ5	Please provide publisher location, editor name for references [Wang et al., 2008].	